Crystallization Behavior of Poly(L-lactic acid) Nanocomposites: Nucleation and Growth Probed by Infrared Spectroscopy

Vahik Krikorian and Darrin J. Pochan*

Department of Materials Science and Engineering and Delaware Biotechnology Institute, University of Delaware, Newark, Delaware 19716

Received April 8, 2005; Revised Manuscript Received May 23, 2005

ABSTRACT: Time-lapsed Fourier transform infrared (FTIR) spectroscopy was employed to probe chain conformational changes during the isothermal crystallization of poly(L-lactic acid), PLLA, and its nanocomposites from the melt. To study the effect of clay exfoliation extent on the crystallization behavior of PLLA, intercalated and exfoliated nanocomposites were fabricated by solution casting two commercially available organoclays with different degrees of matrix miscibility. By solely varying the degree of miscibility between the organic modifier and the polymer matrix, fully intercalated and exfoliated nanocomposites were obtained. This system allowed us to systematically investigate the effect of degree of clay exfoliation on the chain conformational changes during the crystallization process. In the case of neat PLLA, interchain interactions preceded intrachain interactions during the crystallization. Conversely, the exfoliated nanocomposites exhibited an opposite behavior in that 10_3 helix formation and backbone reorientation were followed by the interchain interactions. These results explain the nonnucleating behavior of highly miscible and exfoliated nanocomposites reported in our previous contribution.

Introduction

Crystallization of polymers has been the topic of extensive studies over the past 40 years. While the complicated nature and mechanisms of neat polymer crystallization are fundamentally understood, the addition of an inorganic species into polymeric matrices further increases the complexity of this phenomenon. The interaction of an inorganic phase with the semicrystalline polymer, the volume percent of the interface, shape/dimensions, and surface properties of the inorganic phase can potentially alter the crystallization kinetics, extent of crystallinity, and the crystalline morphology of the organic matrix. In this investigation we attempt to probe the chain conformational changes during the crystallization of a novel nanocomposite system and to elucidate the nucleating properties of the inorganic species with different surface properties and degrees of dispersions. This study was undertaken to also better understand the results reported in our previous contribution,[1] where the intercalated nanocomposites exhibited a significantly faster bulk crystallization kinetics compared to that of the neat matrix and exfoliated nanocomposite. The nanocomposites studied in this work are fabricated by solution casting of neat poly(L-lactic acid) and organically modified clays.

Polymer layered silicate nanocomposites (PLSN) are important due to the fact that they often exhibit enhanced physical and/or chemical properties compared to that of the pure matrix or conventional composites.[2] This enhancement in properties can often be achieved with very low clay loadings where optical clarity is retained making them ideal for many industrial applications. Compatibility between clay platelets and the organic matrix, linked with processing conditions, can drive the system from micron range, phase-separated blends to intercalated and fully exfoliated morphologies. Exfoliated nanocomposites are desirable due to the highest surface-to-volume ratio of filler possible, which gives rise to a larger filler/matrix interface/interphase at a given clay loading.

Environmentally friendly polymers such as poly(lactic acid), PLA, have attracted significant interest in recent years.[3] PLA is a linear, aliphatic, thermoplastic polyester that can undergo enzymatic[4,5] or hydrolytic[6] degradation and is used in the biomedical/pharmaceutical fields.[7] The monomers for PLA synthesis can be produced by fermentation of corn, sugar cane, sugar beat, and potato.[8] Recently, extensive efforts have been made to commercialize PLA in bulk quantities with commercially competitive prices and in a variety of grades. PLA can be produced by ring-opening polymerization of lactides or condensation polymerization of all stereoisomers of lactic acid monomers. A schematic view of the chemical structure of the pure L-stereoisomer, or poly(L-lactic acid) (PLLA), is illustrated in Figure 1.

Despite extensive studies of PLLA, its crystallization behavior and crystal structure are still not completely understood. Depending on the processing conditions, PLLA can crystallize in α, β, or γ forms. Crystallization of PLLA from the melt or from solution under normal conditions results in its most common polymorph, the α form, with a 10_3 helical chain conformation where two chains are interacting in an orthorhombic unit cell.[9,10] Under very high drawing conditions and high temperatures,[10−12] β form crystals are obtained which were first seen in stretched PLLA fibers. The crystal structure of this polymorph is not fully solved although it has been reported that it exists in a 3-fold helical conformation. The β form was considered to have a frustrated structure, containing three chains in the unit cell. Molecular simulations suggest that neither a 3_1 nor a 10_3 helix can reasonably fit the experimental data. Thus, it has been suggested that it exists in a distorted 3_1 helical conformation[13] or frustrated structure with randomly oriented chains.[12] Recently, Cartier et al. have introduced a new polymorph of PLLA by epitaxial growth on hexamethylbenzene.[14] This phase is suggested to contain two antiparallel helices packed in an ortho-

* Corresponding author. E-mail: Pochan@udel.edu.

10.1021/ma050739z CCC: $30.25
Published on Web 06/25/2005

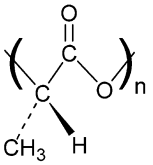

Figure 1. Chemical structure of poly(L-lactic acid) (PLLA).

rhombic unit cell. Therefore, depending on the extent of supercooling, dynamics of the polymer chains, processing, and their microenvironment, PLLA chains can crystallize into different morphologies with different degrees of perfections. The different crystalline morphologies can affect the chemical stability, physical/mechanical properties, and degradation rates[15] in biodegradable polymers. Therefore, a thorough understanding of the crystallization behavior of PLLA is crucial. As a continuation of our previous studies,[1,16] the real-time conformational changes during the crystallization of PLLA and its nanocomposites via Fourier transform infrared (FTIR) spectroscopy are presented.

FTIR is highly sensitive to the conformation and packing density of polymers, making it very useful in crystallization studies of polymers. Characteristic bands can be correlated to the crystalline and amorphous fractions of the bulk and typically stay distinguishable over the course of crystallization. Shape and intensities of FTIR bands are generally susceptible to the temperature at which they are collected. This makes it impractical to controllably study the nonisothermal crystallization behavior of polymers via FTIR, where a constant temperature ramp is applied to the sample. Therefore, the work presented herein is confined to the isothermal crystallization studies of PLLA and its nanocomposites.

Recently, we have demonstrated the relationship between the matrix miscibility of clay organic modifier and the extent of exfoliation and crystallization behavior of final nanocomposites.[16] As the miscibility between the PLLA and the organic modifier was increased, the system displayed a higher degree of exfoliation, resulting in significantly better mechanical properties at given clay loading. In addition, both bulk crystallization behavior and spherulitic growth rate measurements were performed on the neat PLLA vs PLLA/clay nanocomposites.[1] This novel system allowed a direct comparison to be made between the degree of exfoliation and the crystallization behavior of the nanocomposites for both bulk crystallization kinetics and spherulitic radial growth rates. In the case of the least miscible organic modifier, intercalated nanocomposites were obtained where clay acted as a nucleation agent. The final spherulite sizes were considerably smaller than that of neat PLLA with fast bulk crystallization kinetics, similar to conventional filled−polymer systems. However, when the most miscible organic modifier was used, the organoclay was predominantly exfoliated throughout the PLLA matrix. The fully crystallized exfoliated nanocomposites had considerably larger spherulites compared to that of neat PLLA and the intercalated nanocomposite. Not only did the fully exfoliated organoclay not act as a nucleation agent, but it also doubled the spherulitic radial growth rates resulting in a significantly larger spherulitic morphology.

To better understand this phenomenon, conformational changes during crystallization as well as induction period of neat PLLA vs intercalated and exfoliated nanocomposites were observed by time-lapsed FTIR in transmission mode. On the basis of the skeletal and chain conformational changes during isothermal crystallization, the effect of organoclays with different degrees of miscibility on the kinetics of chain conformations was studied. It is shown that during crystallization interchain interactions precede intrachain interactions in the case of both intercalated nanocomposites and the neat polymer while the opposite behavior is seen in exfoliated nanocomposites. This may describe nonnucleating behavior of the organoclay previously seen in fully exfoliated nanocomposites.[1]

Table 1. Characteristics of Organoclays[a]

Clay Type	Extent of Modification [meq/100g clay]	Chemical Structure of Organic Modifier
Cloisite 30B	90	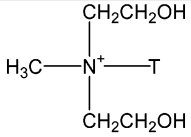
Cloisite 15A	125	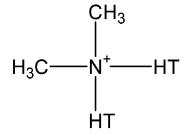

[a] HT is hydrogenated tallow (∼65% C18; ∼30% C16; ∼5% C14).

Experimental Section

Materials. Poly(L-lactic acid) (PLLA) was purchased from Polysciences Inc., Warrington, PA, with a viscosity molecular weight of 325 000−460 000 g/mol as reported by the manufacturer. As-received PLLA was purified by dissolution in chloroform and subsequent precipitation with methanol. Refined polymer was then dried in vacuo for 2 days at 80 °C and kept in desiccation until later use. Two types of organically modified montmorillonite, Cloisite 30B and 15A, were purchased from Southern Clay Product Inc., Gonzales, TX, and used as received. These organoclays are prepared by modification of natural montmorillonite clays with different quaternary ammonium salt. Extent of organic modification and their chemical structures are listed in Table 1 according to the data provided by the supplier. Nanocomposites were prepared by using the solution-intercalation film-casting technique explained elsewhere.[16] The fabricated nanocomposite films were kept under desiccation for future study.

Fourier Transform Infrared Spectroscopy (FTIR). FTIR spectra were collected at 2 cm^{-1} nominal resolution using a Nexus 670 spectrometer (Thermo Nicolet, Madison, WI) with unpolarized light and a MCT detector in transmission mode. The spectra were obtained by averaging 16 scans with a mean collection length of 12 s per spectrum. The background spectra used for reduction were collected at the same temperatures with the sample. The samples were prepared by drop casting a solution of neat PLLA, PLLA loaded with 10 wt % Cloisite 15A (PLLA15A10), and PLLA loaded with 10 wt % Cloisite 30B organoclay (PLLA30B10). The samples were placed in a homemade environmental heating chamber, which was water-cooled to reach the isothermal crystallization temperatures in a short time. Each sample was kept at 200 °C for ca. 10 min to completely melt any possible residual crystalline domains and to erase any thermal history. This was verified by collecting spectra during the heat treatment period. The chamber was purged with nitrogen to both reduce possible thermal degradation of PLLA at elevated temperatures and to reduce the water content in the environment. After completely melting each sample it was cooled to 140 °C in less than 1 min, and the data collection started. Time-resolved FTIR spectra were obtained by collecting each spectrum in 1 min intervals. The frequency regions of interest were trun-

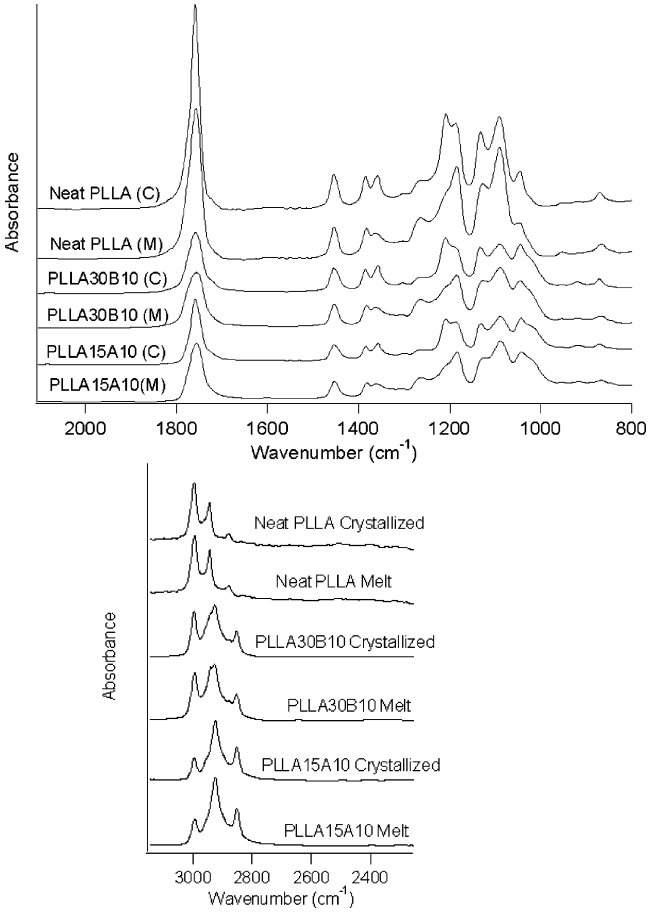

Figure 2. FTIR spectra of the neat PLLA and the nanocomposites in melt and crystallized states: (a) 2000−800 cm^{-1}; (b) 3100−2400 cm^{-1}.

Table 2. Band Assignments of Amorphous and Semicrystalline PLLA

assignment	neat PLLA	PLLA30B10	PLLA15A10
$\nu_{as}CH_3$	2997 m	2997	2997
$\nu_{s}CH_3$	2945 m	2943	2942
$\nu_{as}CH_2$		2926	2924
νCH	2881 w	2881	
$\nu_{s}CH_2$		2854	2852
$\nu C{=}O$	1759 vs	1758	1758
$\delta_{as}CH_3$	1454 s	1454	1454
$\delta_{s}CH_3$	1348−1384 s	1348−1384	1348−1384
$\delta_1 CH + \delta_s CH_3$	1368−1360 s	1368−1360	1368−1360
$\delta_2 CH$	1315−1300 m	1315−1300 m	1315−1300 m
$\delta CH + \nu COC$	1265 s	1262	1263
$\nu_{as}COC + r_{as}CH_3$	1209−1186 vs	1210−1186	1209−1186
$r_{as}CH_3$	1132 s	1132	1131
$\nu_{s}COC$	1090 vs	1090	1088
$\nu C{-}CH_3$	1046 s	1045	1043
$rCH_3 + \nu CC$	960−925 w	960−925	960−925
$\nu C{-}COO$	870 m	871	870
$\delta C{=}O$	756 s	756	756

cated, and the baselines were corrected linearly for each spectrum. The data treatment process was automated by macros written in Igor Pro 4.06 and Thermo Nicolet's software package.

Results

The frequencies and the vibrational assignments for neat PLLA and the nanocomposites are shown in Table 2. These assignments are based on values provided in the literature.[17] Figure 2 shows the spectra of Neat-PLLA, PLLA30B10, and PLLA15A10 both in the quiescent melt state and fully crystallized at 140 °C. All samples exhibit mid-IR regions that are highly sensitive to the structural changes during crystallization: the CH symmetric and asymmetric stretch region of 3200−2800 cm^{-1}, CH, CH_3 bending, and C−O−C stretching band region of 1500−1000 cm^{-1}, and the backbone stretching and CH_3 rocking band region of 960−830 cm^{-1}. In the following sections each of these regions will be discussed separately.

Symmetric and Asymmetric CH Stretching (3200−2800 cm^{-1}). The high wavenumber CH stretching region of neat PLLA and the nanocomposites is shown in Figure 3. No considerable spectral variations can be seen in this region as the crystallization proceeds. However, studying the band shifts in this region provides valuable insight into the molecular conformations of the organic modifiers used in the organoclays. Organic modifiers used in this study are quaternary ammonium salts with aliphatic tails (Table 1) that exhibit methyl- and methylene-related vibrational modes. The bands at approximately 2997 and 2945 cm^{-1} arise from the CH_3 asymmetric and symmetric stretch. These signals are related to both CH_3 groups on the PLLA as well as the organic modifier. However, the bands at approximately 2854 and 2926 cm^{-1}, related to CH_2 symmetric and asymmetric stretch, can be solely attributed to the organic modifiers and are not present in the neat PLLA spectra. Generally, the breadth and the band position of $\nu_{as}CH_2$ are sensitive to the trans/gauche conformer ratio and the packing density of methylene groups.[18] Band shifts from higher to lower frequencies signify a transition from less ordered and more gauche conformations toward more ordered, trans conformations, characteristic of a tightly packed environment. Comparing the asymmetric stretching band of PLLA30B10, 2926 cm^{-1}, to PLLA15A10, 2924 cm^{-1}, it can be concluded that the methylene groups present in the organic modifier of PLLA15A10 have more trans conformations. This is in good accordance with our small-angle X-ray scattering (SAXS) experiments[16] where a predominantly intercalated morphology was reported for PLLA15A10 while PLLA30B10 was fully exfoliated. A similar approach was taken by Vaia et al.[19] where the conformation and molecular environment of interlayer structure in alkylammonium layered silicates were correlated to these characteristic bands.

CH, CH_3 Bending, and C−O−C Stretching Band (1500−1000 cm^{-1}). Figure 4 shows a representative time-resolved spectrum of neat PLLA during crystallization at 140 °C. Similar spectra were obtained for the nanocomposites. Both peak shift and intensity changes can be observed in these spectra. During the course of crystallization, intensities of the crystalline sensitive bands increase while the amorphous-dependent bands decrease. By subtracting the initial spectrum from the consecutive spectra, a difference spectrum can be achieved. For the sake of brevity, only the difference spectra of neat PLLA and PLLA30B10 are shown in Figure 5a,b. The bands in the positive regions are crystalline-dependent peaks while those in the negative regions are amorphous-dependent. Comparing the original spectra with the difference spectra reveals band splitting in some of the regions. For instance, the band at ∼1454 cm^{-1}, which is ascribed to the asymmetric deformation mode of CH_3, is split into two bands at 1458 and 1442 cm^{-1}, where intensities of both increase as the polymer crystallizes. The region of 1300−1000 cm^{-1}, which is mainly related to the C−O−C stretching

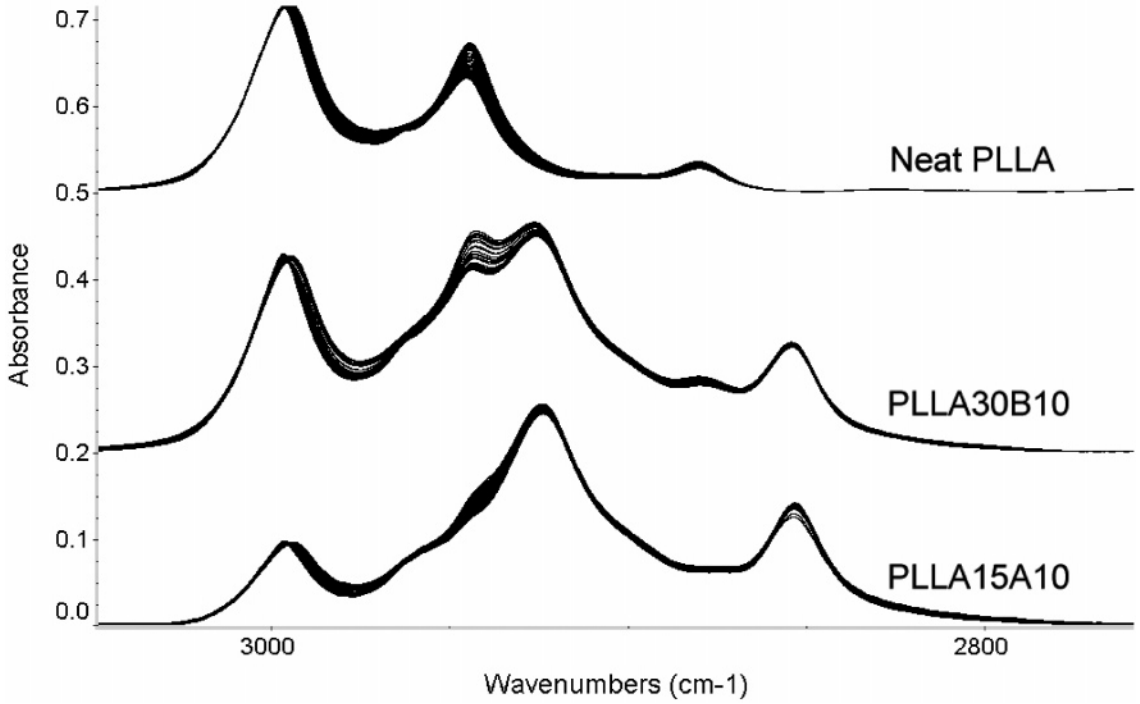

Figure 3. Time-resolved spectra of neat PLLA, PLLA30B10, and PLLA15A10 isothermally crystallizing at 140 °C (3100−2700 cm^{-1}).

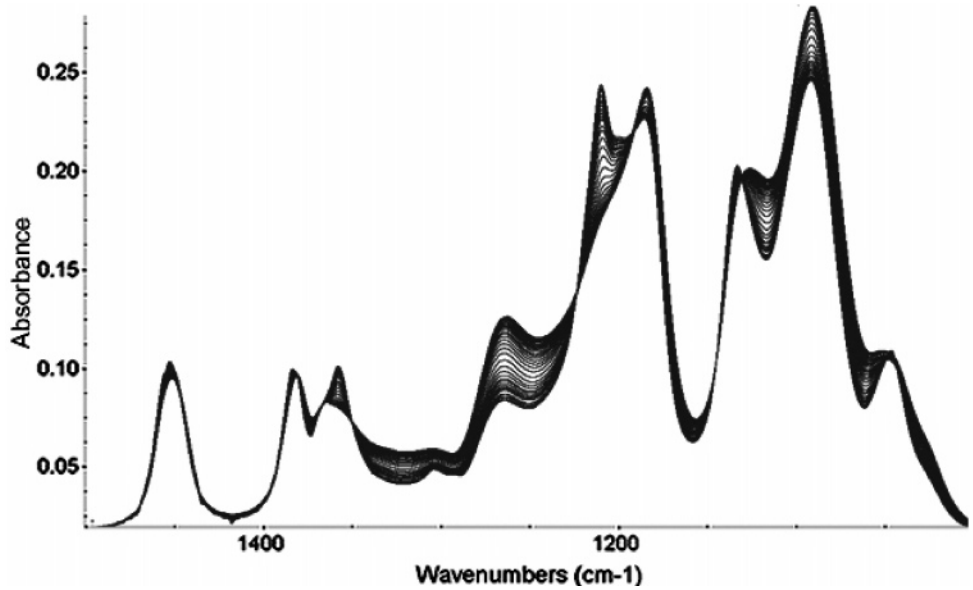

Figure 4. Time-resolved spectra of neat PLLA isothermally crystallizing at 140 °C (1500−1000 cm^{-1}).

vibrations, is also subject to band splitting and peak shifts. For instance, the peak at ~1200 cm^{-1}, attributed to C−O−C asymmetric vibrations linked with asymmetric CH_3 rocking vibrations, shifts to higher wavenumbers with increased intensity. In the difference spectrum this band is split into two peaks at around 1210 and 1180 cm^{-1}.[20]

Backbone Stretching and CH_3 Rocking (960−830 cm^{-1}). This region is sensitive to the degree of crystallinity and the amount of D- or L-isomers in PLLA. Moreover, the band at ~920 cm^{-1} is ascribed to PLLA crystals in the α form with a distorted 10_3 helix conformation,[17,21] arising from the coupling of C−C backbone stretching and the CH_3 rocking mode. Previous experimental and theoretical structure analysis of PLLA has confirmed the existence of considerable amounts of structural disorder within PLLA crystals.[13,21] This structural disorder was suggested to be due to the interchain interactions of CH_3 groups during crystallization.[10]

The time-resolved spectra of neat PLLA for this region are shown in Figure 6. Peak shifting and intensity changes can be observed during the crystallization period. Very similar trends, albeit with different kinetics, can be seen in the nanocomposite systems (data not shown). At the initial stages of the crystallization, no bands can be observed at 920 cm^{-1}, suggesting the absence of crystallinity in the sample. At some point during the crystallization period, this peak becomes visible and its intensity increases until the crystallization is complete. Since the intensity of the other two bands in this region also increases during the crystal-

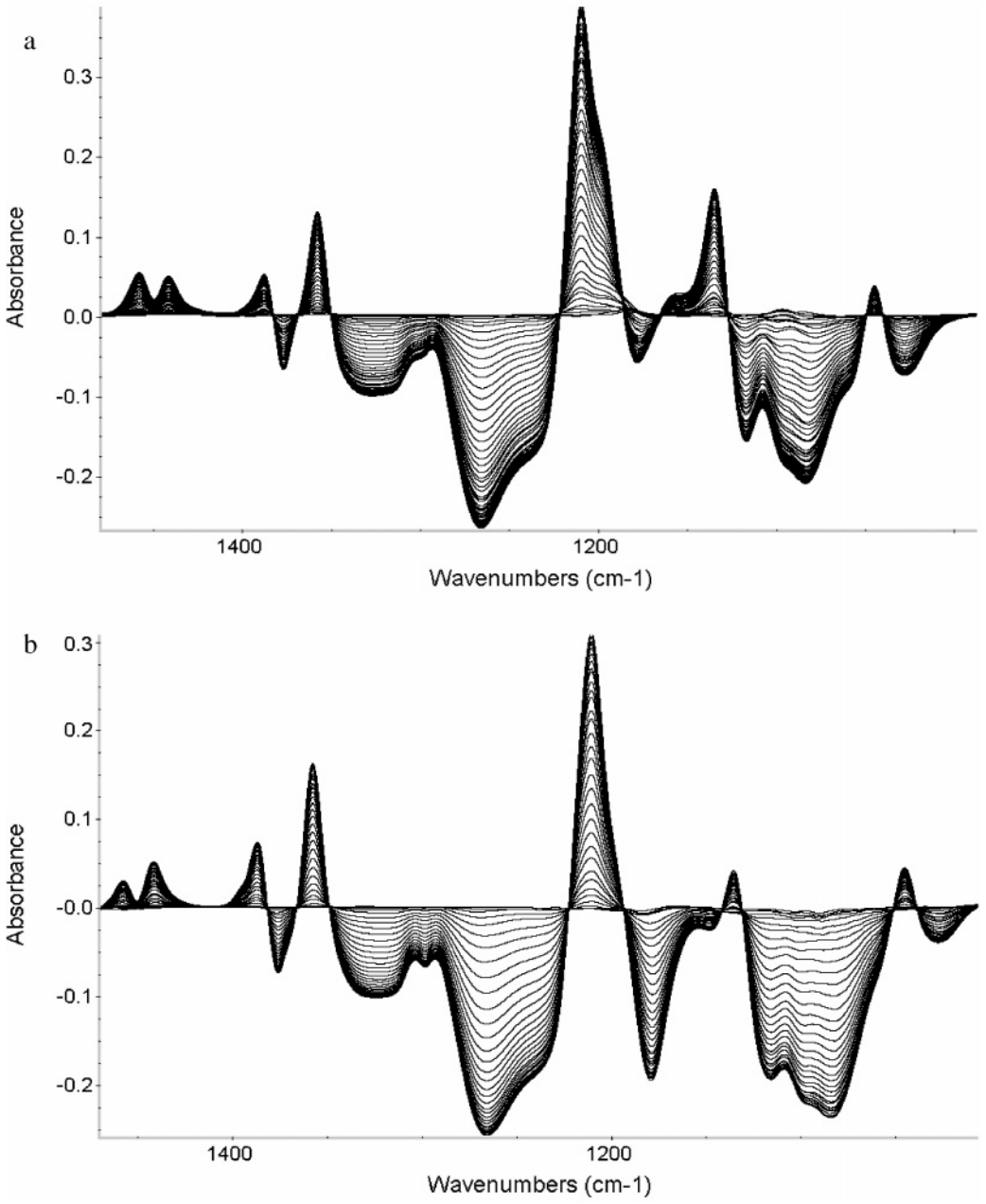

Figure 5. Difference spectra of (a) neat PLLA and (b) PLLA30B10 isothermally crystallizing at 140 °C (1500−1000 cm^{-1}).

lization, they can be assumed to be crystalline-specific bands. The band at ~865 cm^{-1} shifts to the higher wavenumbers, and it becomes sharper during the crystallization process suggesting a transition to a well-defined order.

Discussion

Crystallization Kinetics. To qualitatively compare the variations of 10_3 helix sensitive bands and the skeletal vibrations over the course of crystallization normalized,[22] peak heights of the difference spectra at 1458, 1210, and 920 cm^{-1} are plotted as a function of crystallization temperature (Figure 7a−c). The normalized heights of the peaks at 1458 and 1210 cm^{-1} are used to follow the conformational changes in the backbone while the 920 cm^{-1} band is used to probe the kinetics of 10_3 helix formation. A similar approach has been taken recently by Zhang et al.[23,24] where the kinetics of conformational changes during the crystallization of neat PLLA was investigated. In that work the band splitting of 1458 cm^{-1} was ascribed to the interchain interactions during the formation of 10_3 helical crystal structure caused by CH_3 groups. Our results for neat PLLA are very similar to the neat PLLA results of Zhang et al. However, by applying the same approach to PLLA nanocomposite samples, valuable information regarding the effect of clay platelets with different organic modifiers on the crystallization kinetics of PLLA can be obtained.

Figure 7a−c compares variations of each of these peaks over the crystallization period. Throughout this work we will focus on two characteristics of these sigmoidal curves: (1) the induction time, defined as the time required to detect a considerable increase in conversion relative to the initial stage, and (2) the $t_{1/2}$, or the time at which the crystallization reaches 50% completion. Considering nucleation and growth theory of polymer crystallization, the induction time can be correlated to the nucleation characteristics of the system while the $t_{1/2}$ can be related to the bulk crystallization

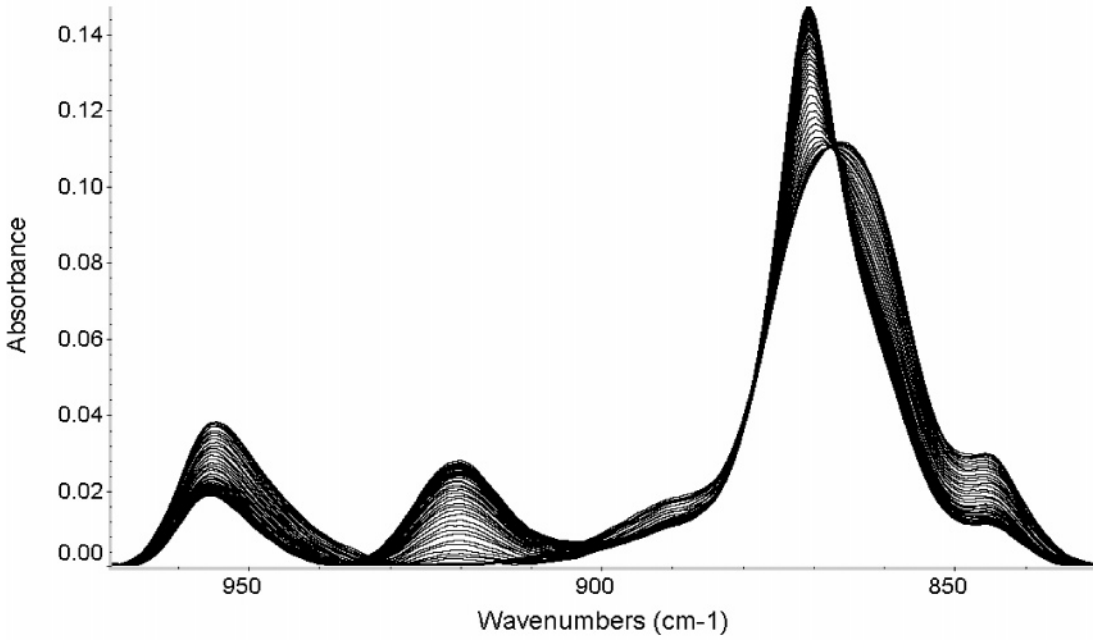

Figure 6. Time-resolved spectra of neat PLLA isothermally crystallizing at 140 °C (1000−800 cm^{-1}).

kinetics. As it is shown in Figure 7a, the induction time for 10_3 helix formation as indicated by 920 cm^{-1} intensity changes for neat PLLA is the largest, followed by PLLA30B10 and PLLA15A10. This suggests that the 10_3 helix formation in the intercalated case starts at significantly earlier stages of the crystallization period while longer times are needed for the neat PLLA and the exfoliated nanocomposites to form stable and detectable helical conformation. We observed similar behavior by DSC where intercalated clay tactoids acted as heterogeneous nucleation sites, significantly lowering PLLA crystallization induction time.[1,25]

The $t_{1/2}$ associated with the intercalated system, PLLA15A10, is the lowest, suggesting faster bulk crystallization kinetics than neat PLLA and PLLA30B10. Figure 7b,c shows the variation of backbone vibrations over the crystallization period and suggests that the induction times for skeletal conformational changes in the case of neat PLLA and the fully exfoliated case, PLLA30B10, are very close, while PLLA15A10 has a short induction time. Overall, the kinetics of these transformations in PLLA15A10 is the fastest.

To compare the interchain interactions and the helix formation kinetics in each sample individually, Figure 8a−c illustrates the same data presented in Figure 7 in a different format. Based on Figure 8a, the induction time for helix formation in neat PLLA, 920 cm^{-1}, is longer than that for skeletal conformational changes signified by the 1207 and 1458 cm^{-1} bands. This suggests that in the case of neat PLLA interchain interactions precede the intrachain helix formation process. This observation is in good agreement with the work of Zhang et al.[23,24] for neat PLLA studied at 150 °C isothermal crystallization temperature. This phenomenon can be linked to a historic debate in the polymer physics field on the mechanism of formation of ordered crystalline regions from a highly entangled melt. In contrast to the Lauritzen−Hoffman approach,[26−28] where the crystallization is assumed to have a nucleation and growth nature and the crystallization is assumed to occur solely on the crystal growth front, there are several other theories which assume a number of metastable steps during the crystallization. These theories range from spinodal decomposition[29] and nucleation followed by growth[30] to Strobl's method.[31] All these methods were developed to describe the formation of ordered structures at very early stages of crystallization observed in several different systems and studied with a wide variety of techniques: from real-time SAXS/WAXS investigations to dielectric spectroscopy.[32−35]

In contrast to neat PLLA, where interchain interactions are detected considerably earlier than intrachain 10_3 helix formation, Figure 8b depicts the opposite behavior for the exfoliated nanocomposite. These data suggest that highly miscible lamellar clay platelets hinder interchain interactions while promoting helix formation. Since interchain interaction is the dominant factor for creation of stable nuclei from the highly entangled melt, this describes the nonnucleating behavior of the fully exfoliated nanocomposite as previously probed by other techniques.[1] The hindrance of interchain interaction can also affect the formation of crystalline domains after the generation of 10_3 helices. This is also in good agreement with the low overall crystallinity of fully exfoliated system, compared to the intercalated nanocomposite and the neat PLLA.[1]

The change of interchain and 10_3 helix sensitive bands for the intercalated nanocomposite are shown in Figure 8c. Compared to the neat PLLA and the exfoliated nanocomposites (Figure 8a,b), both the $t_{1/2}$ and the induction time are very small. On the basis of this figure, resolving the difference between the induction times of each of these individual bands is not possible. This is because of extremely fast crystallization kinetics of this system due to the high nucleating properties of the intercalated clay tactoids.

Conclusion

In the present study we have systematically investigated the effect of high aspect ratio organically modified clays with different degrees of matrix miscibility on the bulk crystallization kinetics of poly(L-lactic acid), PLLA. FTIR spectroscopy was used as a probe of real-time vibrational changes associated with inter- and intra-

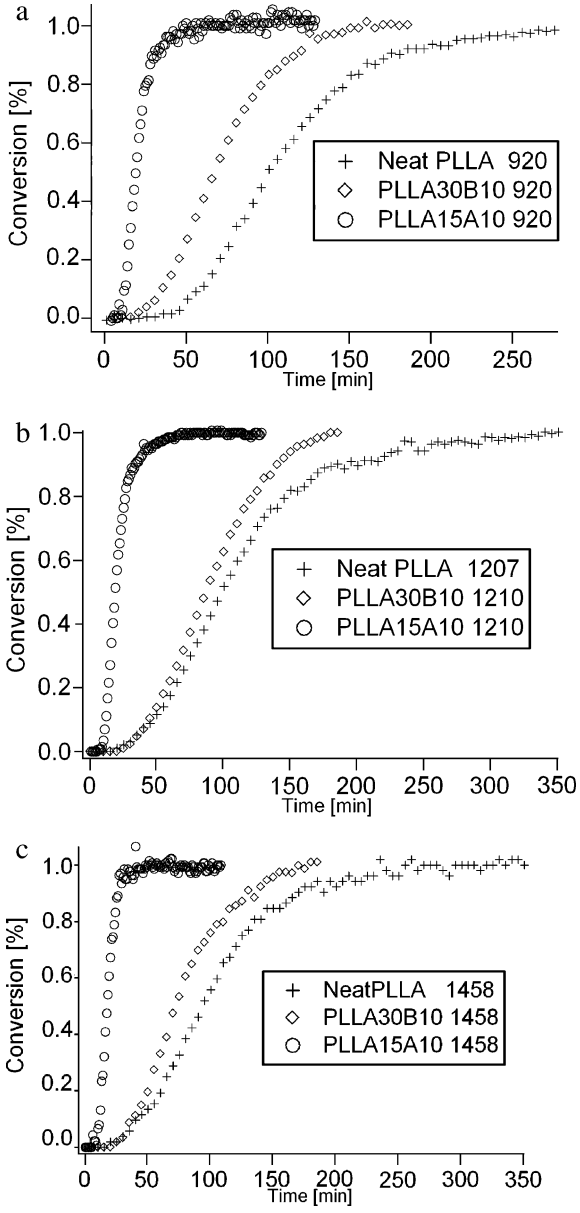

Figure 7. Normalized peak intensities at (a) 920, (b) 1210, and (c) 1458 cm^{-1} as a function of crystallization time for neat PLLA, PLLA15A10, and PLLA30B10.

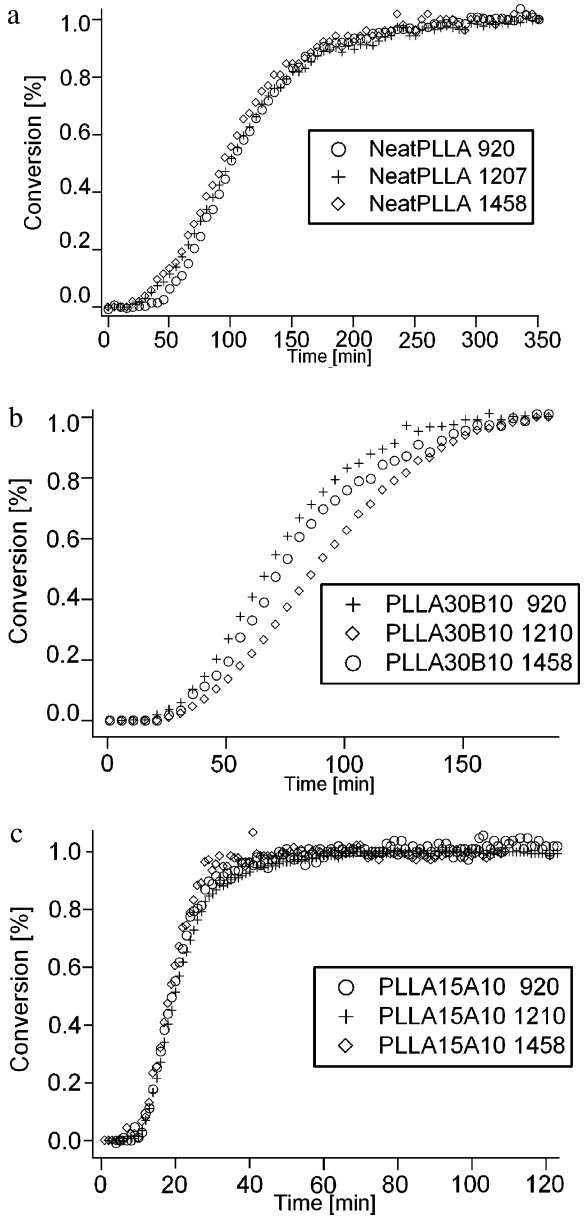

Figure 8. Normalized peak intensities at 920, 1210, and 1458 cm^{-1} as a function of crystallization time for (a) neat PLLA, (b) PLLA15A10, and (c) PLLA30B10.

chain interactions during PLLA crystallization. The spectroscopy results presented herein are complementary to our previous studies[1] and elucidate some of the intriguing aspects of this system that were not clear in our previous approach. In the case of neat PLLA as shown previously by Zhang et al.,[24] interchain interactions preceded that of intrachain and 10_3 helix formation. This is in good accordance with extensive number of reports in the literature where long-range order has been observed notably earlier than the formation of crystalline short-range order from a crystallizing melt.

In the case of intercalated nanocomposites, where less compatible clay tactoids act as nucleation agents, inter- and intrachain interactions started at the same time, and differences in induction times were not possible to resolve. In the case of fully exfoliated nanocomposites, intrachain interactions corresponding to PLLA 10_3 helix formation are observed at significantly earlier stages of the crystallization than interchain interactions. In addition, long lag times were observed in the fully exfoliated case, where the mean distance between adjacent lamellar clay sheets is comparable to the radius of gyration of the high molecular weight PLLA. Highly miscible clay hinders the interchain interactions vital for crystal nuclei formation. The 10_3 helix formation preceding interchain interactions describes the nonnucleating behavior of the fully exfoliated nanocomposite reported previously.

Acknowledgment. V.K. is grateful to Prof. John F. Rabolt for use of the FTIR spectrometer and Yujuan Liu for her assistance. This work was partially supported by the National Science Foundation Career Award DMR-0348147 and NSF-NIRT DMR-0210223.

References and Notes

(1) Krikorian, V.; Pochan, D. J. *Macromolecules* **2004**, *37*, 6480−6491.
(2) Alexandre, M.; Dubois, P. *Mater. Sci. Eng., R* **2000**, *28*, 1−63.
(3) Ikada, Y.; Tsuji, H. *Macromol. Rapid Commun.* **2000**, *21*, 117−132.
(4) Tsuji, H.; Ikada, Y. *J. Appl. Polym. Sci.* **1998**, *67*, 405−415.

(5) Sinclair, R. G. *J. Macromol. Sci., Pure Appl. Chem.* **1996**, *A33*, 585−597.
(6) Iwata, T.; Doi, Y. *Macromolecules* **1998**, *31*, 2461−2467.
(7) Edlund, U.; Albertsson, A. C. In *Degradable Aliphatic Polyesters*; Springer, Berlin, 2002; Vol. 157, pp 67−112.
(8) Kharas, G. B. S.-R. F.; Severson, D. K. *Plastics From Microbes*; Hanser Publishers: New York, 1994.
(9) Desantis, P.; Kovacs, A. J. *Biopolymers* **1968**, *6*, 299.
(10) Hoogsteen, W.; Postema, A. R.; Pennings, A. J.; Tenbrinke, G.; Zugenmaier, P. *Macromolecules* **1990**, *23*, 634−642.
(11) Eling, B.; Gogolewski, S.; Pennings, A. J. *Polymer* **1982**, *23*, 1587−1593.
(12) Puiggali, J.; Ikada, Y.; Tsuji, H.; Cartier, L.; Okihara, T.; Lotz, B. *Polymer* **2000**, *41*, 8921−8930.
(13) Brizzolara, D.; Cantow, H. J.; Diederichs, K.; Keller, E.; Domb, A. J. *Macromolecules* **1996**, *29*, 191−197.
(14) Cartier, L.; Okihara, T.; Ikada, Y.; Tsuji, H.; Puiggali, J.; Lotz, B. *Polymer* **2000**, *41*, 8909−8919.
(15) Reed, A. M.; Gilding, D. K. *Polymer* **1981**, *22*, 494−498.
(16) Krikorian, V.; Pochan, D. J. *Chem. Mater.* **2003**, *15*, 4317−4324.
(17) Kister, G.; Cassanas, G.; Vert, M. *Polymer* **1998**, *39*, 267−273.
(18) Snyder, R. G.; Strauss, H. L.; Elliger, C. A. *J. Phys. Chem.* **1982**, *86*, 5145−5150.
(19) Vaia, R. A.; Teukolsky, R. K.; Giannelis, E. P. *Chem. Mater.* **1994**, *6*, 1017−1022.
(20) In general, if the intermolecular interactions between polymeric chains are significant, their fundamental modes of vibrations are split into different components.
(21) Kang, S. H.; Hsu, S. L.; Stidham, H. D.; Smith, P. B.; Leugers, M. A.; Yang, X. Z. *Macromolecules* **2001**, *34*, 4542−4548.
(22) The intensity of each of these peaks was normalized to their final intensity after the crystallization was reached to the final completion.
(23) Zhang, J. M.; Tsuji, H.; Noda, I.; Ozaki, Y. *Macromolecules* **2004**, *37*, 6433−6439.
(24) Zhang, J. M.; Tsuji, H.; Noda, I.; Ozaki, Y. *J. Phys. Chem. B* **2004**, *108*, 11514−11520.
(25) It should be noted that this approach only describes the crystallinity index and not the absolute crystallinity of the samples probed by other techniques, e.g., DSC. Moreover, vibrational changes probed by FTIR are not necessarily coming from three-dimensional ordering during the crystallization; they can be due to two-dimensional interactions as well.
(26) Hoffman, J. D.; Weeks, J. *J. Res. Natl. Bur. Stand., Sect. A* **1962**, *66*, 13.
(27) Hoffman, J. D. *Polymer* **1982**, *23*, 656−670.
(28) Hoffman, J. D. *Polymer* **1983**, *24*, 3−26.
(29) Olmsted, P. D.; Poon, W. C. K.; McLeish, T. C. B.; Terrill, N. J.; Ryan, A. J. *Phys. Rev. Lett.* **1998**, *81*, 373−376.
(30) Muthukumar, M.; Welch, P. *Polymer* **2000**, *41*, 8833−8837.
(31) Strobl, G. *Eur. Phys. J. E* **2000**, *3*, 165−183.
(32) Wurm, A.; Soliman, R.; Schick, C. *Polymer* **2003**, *44*, 7467−7476.
(33) Wang, Z. G.; Hsiao, B. S.; Sirota, E. B.; Agarwal, P.; Srinivas, S. *Macromolecules* **2000**, *33*, 978−989.
(34) Pogodina, N. V.; Siddiquee, S. K.; van Egmond, J. W.; Winter, H. H. *Macromolecules* **1999**, *32*, 1167−1174.
(35) Wang, Z. G.; Hsiao, B. S.; Sirota, E. B.; Srinivas, S. *Polymer* **2000**, *41*, 8825−8832.

MA050739Z